An Investigation of the Quantum Chemical Description of the Ethylenic Double Bond in Reactions: II. Insertion of Ethylene into a Titanium–Carbon Bond

VIDAR R. JENSEN, KNUT J. BØRVE

Department of Chemistry, University of Bergen, Allégaten 41, 5007 Bergen, Norway

Received 9 September 1997; accepted 18 January 1998

ABSTRACT: Insertion of ethylene into the Ti–methyl bond in $TiH_2CH_3^+$ is chosen as a model reaction for investigating the performance of a range of contemporary quantum chemical models in polymerization studies. Basis set effects are investigated at the self-consistent-field level, covering Hartree–Fock, pure DFT, and hybrid DFT. In agreement with findings in part I of this study, the basis set sensitivity of ethylene is shown to introduce a bias in computed energetics, amounting to 2–3 kcal/mol when DZP bases are used to compute the overall heat of monomer insertion. The geometry of stationary points relevant to the insertion reaction is determined using hybrid density functional theory. Based on these structures, the energy profile of the insertion reaction is computed using a range of popular quantum chemical approximations. The methods include Hartree–Fock and Møller–Plesset (MP) perturbation theory up through the fourth order in spin-restricted, spin-unrestricted, and spin-projected formalisms. Furthermore, configuration-interaction-based methods are included, of which the top level method is singly and doubly excited coupled clusters with a perturbative estimate of the contribution from triply excited configurations added [CCSD(T)]. The performance of the methods just mentioned, as well as three pure density functional and three hybrid density functional methods, are compared with respect to ''best'' relative energies, defined through extrapolation of CCSD(T) correlation energies according to the PCI scheme of Siegbahn and coworkers. Even though the MP series show poor

Correspondence to: K. J. Børve

Contract/grant sponsor: Norwegian Academy of Science and Letters and Statoil, through the VISTA program

CCC 0192-8651 / 98 / 080947-14

convergence, spin-projected MP2, as well as two pure DFT methods (BPW91, BP86) and PCI-78 based on the MCPF method, show similar and very good agreement with best relative energies for the insertion reaction. © 1998 John Wiley & Sons, Inc. J Comput Chem 19: 947–960, 1998

Keywords: olefin polymerization; Ziegler–Natta catalysis; quantum chemical methods; ethylene; $TiH_2CH_3^+$

Introduction

As detailed in part I of the present study,[1] the ethylenic functional group is of utmost importance in many organic and organometallic chemical reactions. Polymerization undoubtedly constitutes one of the classes of reactions that receives most attention, also from a theoretical point of view. Quantum chemical modeling has become a standard tool for investigation of transition-metal-catalyzed ethylene polymerization. A number of such studies are published each year (see, e.g., refs. 2–6, and references therein), sometimes with different conclusions reached for the same chemical system as a result of different methods and basis sets. An example can be found in the study by Yoshida et al.,[7] who examined the relatively high barriers to insertion, obtained using quadratic configuration interaction with single and double substitutions of the Hartree–Fock reference (QCISD) with split-valence basis sets, as compared with those obtained by several other investigators.[8–11] In particular, Yoshida et al. pointed out differences from the results obtained with density functional theory (DFT) and second order perturbation theory (MP2), but concluded that more sophisticated calculations are needed to obtain accurate estimates of the insertion barrier. Axe and Coffin,[12] comparing results of ethylene insertion using second order perturbation theory and gradient-corrected DFT as their most accurate methods, also concluded that more thorough correlation treatment is needed. In addition, the latter investigators suggested that a broader comparison of the performance of various density functionals on ethylene insertion reactions should be performed. Unfortunately, the number of atoms involved in most catalytic systems makes it exceedingly expensive to perform calculations accurate enough to serve as calibration in such studies. Comparison to experimental results cannot solve this problem as it is not even clear which elementary reaction step is responsible for the measured activation energy. The use of a small model of the active catalyst was thus considered imperative, as the main goal of the present study is to treat the electronic effects of a simple chain propagation step accurately enough to evaluate the performance of a series of contemporary quantum chemical methods.

To this end, we have chosen to carry out detailed and accurate calculations of ethylene insertion into the metal–methyl bond in $TiH_2CH_3^+$, which may be viewed as a model of the active species in a Ziegler–Natta catalyst for olefin polymerization. The system is also of relevance to modern single-site catalysts, in which alkyl cations of the general kind MCp_2R^+ (M = Ti, Zr) have been identified as the active catalytic species.[13–15] In several earlier theoretical studies,[11,16,17] chlorides have been used successfully in replacement of the cyclopentadienyl anions, and the present use of hydride ligands may be viewed as a further simplification. The use of Ti instead of Zr as the active metal was motivated by the fact that first-row transition metals generally constitute a more serious theoretical challenge due to the $3d$ and $4s$ orbitals being rather similar in size and, as such, is expected to afford better discrimination among the quantum chemical methods.

Most theoretical studies have followed a direct insertion mechanism, close to that proposed by Cossee,[18] and the calculations have confirmed that this route should constitute a feasible reaction with a low activation energy. According to this mechanism, a propagation step is initiated by the coordination of a monomer onto a vacant site on the metal complex that holds at least one alkyl ligand. The monomer subsequently inserts into the metal–alkyl bond via a four-center transition state involving the alkyl group, the alkene, and the transition metal. In quantum chemical studies, it is generally found that agostic interactions are present in several of the intermediate structures. Typically, an agostic interaction from a hydrogen atom attached to the α carbon of the polymer chain is found to enhance insertion, in line with suggested modifications of the Cossee mechanism.[19–21]

The direct insertion mechanism will also be followed in the present study. Emphasis is put on

the quantum chemical description of geometry, electronic structure, and energy of stationary points along the route of ethylene insertion into the metal–methyl bond in $TiH_2CH_3^+$. This study is concerned with basis set requirement and the performance of a number of contemporary quantum chemical methods in the description of this reaction. The methods include Møller–Plesset perturbation theory up through the fourth order, configuration-interaction-based methods, as well as a series of density-functional-theory-based methods.

Computational Details

BASIS SETS

Calculations were performed using spherical harmonics bases, expect when the ANOM and 6-31G(d, p) bases (see subsequent text) were used in conjunction with the Hartree–Fock method. For the latter calculations, Cartesian bases including the s component of d-shells and the three p components of f-shells were used. Each of the basis sets used in the current work is listed in what follows, along with a short description. Contraction schemes are detailed in Table I.

6-31G(d, p). Our standard basis sets for geometry optimization were a combination of the 6-31G(d, p) sets by Pople and coworkers[22,23] for the ligands, and a titanium basis prepared by contracting the primitive set reported by Wachters[24] in a general manner.[25,26] Flexibility in the outer valence was provided by splitting off the outer s and d exponents, and adding two primitive $4p$ exponents and a diffuse d exponent ($\alpha_d = 0.072$).

ANOS. Our smallest atomic natural orbital (ANO) bases were used in energy calculations. For nonmetal atoms, they were prepared as general contractions of Huzinaga primitive bases,[27] with the addition on a single set of primitive polarization functions ($\alpha_d = 0.63$ for carbon, $\alpha_p = 0.8$ for hydrogen). Titanium was described as detailed previously, except for the addition of a $(3f)/[1f]$ polarization function.[28]

TZD2P. These sets make up our standard sets for energy calculations. For carbon, a Huzinaga primitive $(10s6p)$ basis[27] contracted to $[5s3p]$[29] and augmented with two d functions ($\alpha_d = 1.299$, 0.433) was used. Diffuse s and p functions were added in an even-tempered manner. Hydrogen was described by a scaled (factor 1.49) Huzinaga primitive $(5s)$ set[27] contracted to $[3s]$.[29] Basis sets for the two hydrogen atoms directly attached to titanium were augmented by a single set of p functions ($\alpha_p = 1.0$), whereas two sets ($\alpha_p = 1.7$, 0.6) were added for the rest of the hydrogens. For titanium, the primitive basis is identical to what was detailed for ANOS. However, the contraction of the innermost $(14s9p4d)$ functions follows Wachter's scheme 3. The two outermost d exponents are left uncontracted, and two contracted f functions are prepared from the same primitive $(3f)$ set[28] as for ANOS noted earlier.

ANOM. Pierloot et al.[30] prepared a range of medium-sized ANO sets, which in this work are used to investigate basis set effects at the HF level. Based on our experience from part I of this study, the ANOM bases are expected to provide useful estimates of the Hartree–Fock limit energy differences.

METHODS

The chemical system under study consists of only closed-shell molecules, and, in general, restricted determinants were used to form wave functions. However, some calculations were performed using unrestricted Hartree–Fock (UHF) and perturbation theory based on an UHF reference state (UMPn), as well as spin projections of these wave functions. In all DFT calculations, the density was evaluated using a grid with 75 radial

TABLE I.
Basis Set Contractions Used for Calculating Ethylene Insertion in $TiH_2CH_3^+$.

Basis[a]	Ti	C	H
6-31G(d, p)	$(14s11p6d)$ / $[5s4p3d]$	$(10s4p1d)$ / $[3s2p1d]$	$(4s1p)$ / $[2s1p]$
ANOS	$(14s11p6d3f)$ / $[5s4p3d1f]$	$(9s5p1d)$ / $[3s2p1d]$	$(5s1p)$ / $[3s1p]$
TZD2P	$(14s11p6d3f)$ / $[8s6p3d2f]$	$(11s7p2d)$ / $[6s4p2d]$	$(6s2p)$ / $[3s2p]$[b]
ANOM	$(17s12p9d4f)$ / $[8s7p7d4f]$	$(10s6p3d)$ / $[7s6p3d]$	$(7s3p)$ / $[4s3p]$

[a] The ANO sets are generally contracted,[25,26] whereas the other sets are segmented.
[b] The two hydrogen atoms directly attached to titanium are described by $(6s1p)$ set contracted to $[3s1p]$.

shells per atom and 302 angular points per shell. Relativistic effects were estimated by first-order perturbation theory and found to be negligible, thus omitted.

Geometry Optimizations

All stationary points were characterized by the curvature of the potential energy surface (PES). All geometry optimizations and Hessian calculations at the HF level of theory were performed using the GAMESS set of programs.[31] Geometries were converged to a maximum gradient below 10^{-5} a.u.

Geometry optimizations including the effects of electron correlation were performed using the hybrid density-functional-theory method denoted by B3LYP, to be described in what follows. The Gaussian-94 set of programs[32] was used for this purpose, with convergence criteria set to maximum gradient and displacement of $4.5 \cdot 10^{-4}$ a.u. and $1.8 \cdot 10^{-3}$ a.u., respectively.

Energy Evaluation

Single-point energy calculations were performed at the HF level as well as with a series of methods that include electron correlation. Among the latter methods are density functional theory (DFT), configuration interaction (CI), and many-body perturbation theory. All valence electrons were correlated in the CI and perturbation theory calculations. In addition, estimates of core-correlation effects were computed as detailed later, and added when indicated. Each of the methods are described briefly in the following.

MPn. Perturbation theory was applied in terms of Møller–Plesset (MP) theory[33] to the second, third, and fourth order, using both a restricted (RMPn) and unrestricted (UMPn) formalism. Furthermore, spin contaminants of spin quantum numbers 1–4 were projected out of the UMPn expressions, to give PMPn results. The symbol MP4SDQ is used to denote fourth order Møller–Plesset without triples, which is a frequently used approximation to full MP4. The MPn calculations were performed by means of the Gaussian-94 set of programs.[32]

MCPF. The modified coupled pair functional (MCPF) method[34] is a size-consistent, single-reference-state method. The zeroth order wave functions were defined at the RHF level. The MCPF calculations were performed using the STOCKHOLM[35] sets of programs.

CCSD(T). The most accurate of the CI methods applied here is expected to be coupled cluster[36] with single and double substitutions[37–40] of the HF reference along with a perturbative estimate of connected triples [CCSD(T)].[41] CCSD and CCSD(T) calculations were performed by means of the Gaussian-94 set of programs.[32]

PCI-*X*. Scaling of the correlation energy has been adopted as a scheme for obtaining accurate estimates of relative energies in the present study. The strategy used is the PCI-*X* scheme according to Siegbahn et al.,[42] where X is the percentage of the correlation effects that the parent CI method is expected to account for. The PCI-*X* scheme was originally developed for scaling of correlation energies obtained with the MCPF method and with bases of ANOS (see earlier) quality, for which the optimal value of X was found to be close to 78.[43] An improved estimate of relative energies is thus obtained by adding 22% of the difference between the SCF energy and the total extrapolated energy. With basis sets comparable to TZD2P in quality, X increases to 81,[43] still referring to the MCPF method. The corresponding scaling factor appropriate for CCSD(T) in conjunction with TZD2P bases is given by $X = 85 \pm 3$, as discussed in ref. 44.

The rest of the methods are either based solely on DFT or are hybrids of DFT and HF. They will be referred to by abbreviations denoting the exchange and correlation functionals used in each case, to be detailed in what follows. All corresponding calculations were performed with the Gaussian-94 set of programs.[32]

LSDA. Local correlation and exchange were accounted for in the local spin-density approximation (LSDA, often termed simply LDA) calculations, using Slater exchange,[45] and a correlation functional fitted to the RPA solution of the uniform electron gas by Vosko et al.,[46] conventionally termed VWN.

BLYP, BP86, BPW91. Gradient corrections to the exchange functional were included in terms of the 1988 exchange functional of Becke,[47] denoted by the capital letter B. Gradient-corrected correlation functionals were included either in terms of the 1988 correlation functional by Lee et al.,[48] or the local correlation functional of Perdew (1981) in combination with his 1986 gradient corrections,[49] or the correlation functional from 1991 by Perdew and Wang.[50] These correlation functionals are denoted by LYP, P86, and PW91, respectively.

B3LYP, B3P86, B3PW91. Three different hybrid DFT methods have been employed, differing

mainly in the choice of nonlocal corrections to the local correlation functional, which is taken to be VWN (described earlier). The nonlocal correlation corrections are chosen among those described previously. In each case, the exchange functional contains contributions from the 1988 exchange functional of Becke,[47] as well as HF and Slater exchange terms. The contribution of each functional in the resulting exchange and correlation functional is taken from the work of Becke on a closely related three-parameter hybrid functional, B3. Accordingly, these methods are denoted by the prefix B3 and a suffix native to the nonlocal correlation functional used.

CORE-CORRELATION EFFECTS

To qualify the performance of the various computational methods employed in this study, a highly accurate energy profile is required for the reaction in question. As stated already, we will rely on CCSD(T) energies, extrapolated according to the PCI-85 scheme to include the effects of higher excitations and extension of the one-particle bases, to constitute our most accurate valence-correlated numbers. However, DFT and hybrid HF–DFT methods include even core–core and core–valence correlation. Hence, to provide a fair comparison, our best estimates should include these higher order effects. Due to similarity in radial extension between Ti $3s$, p and Ti $3d$, the outer core of titanium is responsible for the main part of the core–valence and core–core correlation effects. Correlating core electrons is a notorious problem in *ab initio* quantum chemistry. In some systems it may be solved by resorting to the semiclassical core-polarization operator formalism,[51] but this approach does not seem very promising for the early first-row transition metals.[52] Thus, here correlation of the titanium outer core is addressed by conventional CI and perturbational methods, with particular attention paid to basis set superposition errors (BSSE). In what follows, any effect of core correlation is reported relative to free reactants.

First, core correlation effects were computed for the transition state, using both MCPF and CCSD(T) in conjunction with the TZD2P bases. Very similar stabilization of the transition state was obtained with the two methods, giving 5.2 and 4.8 kcal/mol, respectively. This suggests that, for the present system, MCPF is capable of providing core correlation estimates of nearly the same quality as is CCSD(T). Accordingly, all subsequent CI-based estimates of the effect of core correlation are computed by means of MCPF, which is a substantially less resource demanding method than CCSD(T).

Second, the titanium basis was improved by decontracting the outer $3p$ function, originally made up by a $[2p]$ contraction, and reducing the degree of contraction in the $(6d)$ set to 3111. The innermost of these functions, consisting of the $[3d]$ contraction, has its radial maximum near those of $3s$ and $3p$. Even though this represents a modest improvement of the TZD2P bases, the demand on computer resources soars. Energetically, the basis set effect is to reduce the stabilization of the transition state by 1.0 kcal/mol relative to free reactants. This is probably due to a reduction in BSSE, and BSSE may still be responsible for a significant portion of the net 4.2-kcal/mol core-correlation-induced stabilization of the TS retained with this extended basis set.

Third, numerical values of the BSSE were computed using MCPF/TZD2P and the counterpoise method. It was decided to compute BSSE only for the π-complex, where it is straightforward to define the two interacting fragments. A computed core-correlation-induced stabilization of the π-complex of 3.0 kcal/mol is reduced by 1.2 kcal/mol according to the counterpoise method. It is likely that BSSE will increase as the ethylene moiety gets closer to the metal, such as that found in the transition state. Thus, although it is impractical to compute BSSE at each stationary point along the reaction profile, the BSSE content of the π-complex allows an estimation of the BSSE associated with core correlation as being a fraction of $1.2/3.0$ $(= 0.4)$ of the computed core-correlation energy. According to the PCI-X strategy discussed earlier, the thus obtained correlation effects may by trusted to include some 81% of the true core-correlation effects. Hence, our final estimates of the core-correlation effects are taken to be $60\%/0.81$ of their nominal values obtained by MCPF using TZD2P bases. Relative to free reactants, the BSSE-corrected estimates are given by -2.2, -3.9, -3.3, -1.7, and -0.8 kcal/mol for the π-complex, transition state, γ-,β-, and nonagostic product, respectively.

A similar procedure was used to obtain core-correlation effects at the MP2 level of accuracy. Computed core-correlation energies, obtained using the restricted formalism, were scaled by $(2.3 - 1.1)/2.3$, based on a computed BSSE of 1.1 kcal/mol and an uncorrected core-correlation en-

ergy of 2.3 kcal/mol for the π-complex (relative to free reactants). The final BSSE-corrected estimates of core-correlation effects at the MP2 level of accuracy are given by -1.2, -3.0, -2.3, -1.0, and -0.4 kcal/mol for the π-complex, transition state, γ-, β-, and nonagostic product, respectively.

Results and Discussion

CORRELATION AND BASIS SET EFFECTS ON GEOMETRY PARAMETERS

Initially, three methods were selected as geometry generators in the present project, namely Hartree–Fock (HF), the local spin-density approximation (LDA), and the gradient-corrected hybrid density functional theory (DFT) method termed B3LYP (cf. ''Computational Details''). However, as no π-complex could be located with the LDA method, only geometries obtained with HF and B3LYP, using carbon and hydrogen 6-31G(d, p) bases, are reported here. Furthermore, ethylene was found to insert directly and without activation into a titanium–hydride bond when approaching in a perpendicular orientation to the Ti-methyl bond. This reaction channel was not considered relevant in the present study.

Five different stationary points were located along the route of direct insertion of ethylene into the metal–methyl bond. The structures optimized with B3LYP are shown in Figure 1: the reactant $TiH_2CH_3^+$ (upper left); the π-complex (upper right); the transition state of insertion (middle left); a γ-agostic product (middle right); and a β-agostic product (bottom left). No α-agostic product was located. However, a third product structure with only negligible agostic interactions (α) was constructed by rotating the end-ethyl group of the γ-agostic product 180° about C_1-C_2. Cs symmetry was maintained and the parameter $\angle TiC_1C_2$ fixed at 109.5° in the subsequent optimization. C_1 and C_2 are the ethylenic carbon atoms, with C_1 being bound to Ti in the products. Thus, the bottom right structure of Figure 1 does not represent a minimum on the potential energy surface (PES), and is only included to illustrate effects from agostic interactions specific to the product structures.

In Table II, selected geometry parameters optimized at the B3LYP level of accuracy are reported, with deviations to the corresponding HF-optimized structures given within parentheses. Whereas experimental structural data are available for comparison only for ethylene itself, the close

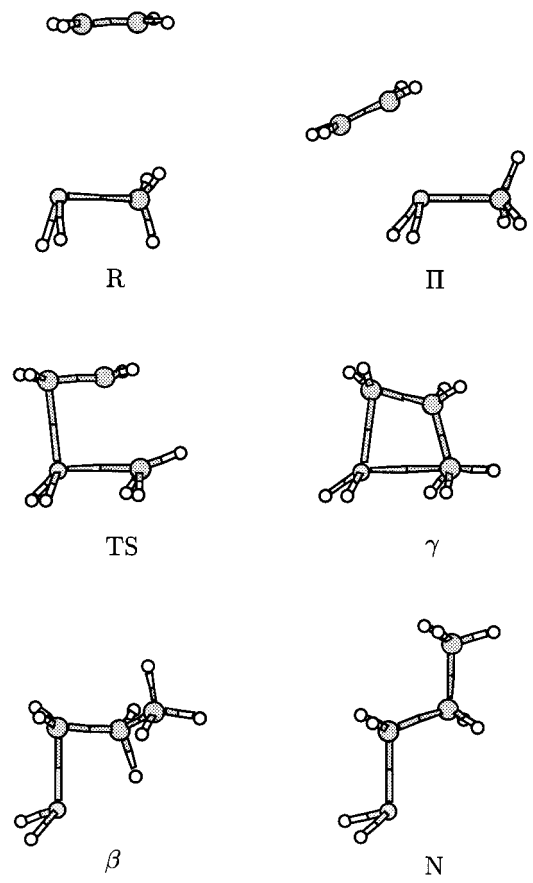

FIGURE 1. Stationary points of ethylene insertion into the Ti-C bond in $TiH_2CH_3^+$ as optimized at the B3LYP level: reactant $TiH_2CH_3^+$ (upper left); π-complex (upper right); the transition state (middle left); the γ-agostic product (middle right); the β-agostic product (bottom left); and the nonagostic product (bottom right). The latter structure, which does not represent a minimum on the PES, was constructed by rotating the end-ethyl group of the γ-agostic product 180° about C_1-C_2. Cs symmetry was maintained and the angle $\angle TiC_1C_2$ fixed at 109.5° in the subsequent optimization. C_1 and C_2 are the ethylenic carbon atoms, with C_1 being bound to Ti in the products.

agreement between B3LYP and QCISD geometries in part I of the present study[1] suggests that B3LYP is able to provide accurate structures.

Generally, the differences between the HF- and B3LYP-optimized geometries are minor and mainly associated with secondary ligand–metal interactions. This can be shown by examining the orientation of the methyl moiety. In the reactant, the orientation is determined by repulsion to the hydride ligands, resulting in a staggered conformation. When the ethylene monomer approaches titanium and the methyl ligand, repulsion between hydrogen atoms in the two organic ligands be-

TABLE II.

Selected Geometry Parameters [Å] Optimized by B3LYP for Reactants, π-Complex, Transition State (TS), and Three Conformations of the Product of Ethylene Insertion in $TiH_2CH_3^+$.

Parameter	Reactants	π-Complex	TS	γ-Agostic	β-Agostic	Nonagostic[a]
$R(TiC_1)$		2.686 (1.1)[b]	2.142 (−2.4)	1.964 (0.3)	1.971 (0.7)	1.948 (3.2)
$R(TiC_2)$		2.507 (16.8)	2.494 (0.1)	2.394 (10.8)	2.438 (3.0)	2.855 (3.0)
$R(TiC_3)$	1.965 (3.0)	1.976 (2.9)	1.974 (6.3)	2.190 (13.9)	3.564 (5.9)	4.278 (2.1)
$R(C_1C_2)$	1.331 (−1.5)	1.352 (−1.5)	1.393 (1.0)	1.550 (0.2)	1.521 (0.4)	1.536 (0.2)
$R(C_2C_3)$		3.618 (6.0)	2.325 (−10.0)	1.608 (−2.5)	1.533 (−0.2)	1.548 (−1.0)
$R(TiH_{agostic})$	2.528 (2.5)	2.497 (8.2)	2.102 (9.6)	2.174 (10.8)	2.033 (4.6)	2.460 (4.8)
$\delta R_{agostic}$[c]	0.003 (0.2)	0.004 (−0.1)	0.035 (−0.4)	0.026[d] (−0.3)	0.062 (0.0)	0 (0.0)

[a]This conformation was constructed by rotating the end-ethyl group of the γ-agostic product 180° around C_1-C_2, maintaining Cs symmetry and freezing $\angle TiC_1C_2 = 109.5°$ in the optimization. Thus, the structure does not represent a minimum on the PES.
[b]The deviation between HF- and B3LYP-optimized distances are given in pm within parentheses following each B3LYP value. A positive deviation implies a longer bond distance at the HF level of accuracy than obtained by means of B3LYP.
[c]$\delta R_{agostic} = \overline{R(CH_{agostic})} - \overline{R(CH)}$.
[d]Two agostic hydrogens.

comes increasingly important. At the transition state both HF and B3LYP predict the methyl moiety to be staggered to ethylene, and, consequently, eclipsed to TiH_2. However, for the π-complex, B3LYP predicts a closer approach of ethylene than does HF, as is evident by differences of 17 and 6 pm in the TiC_2 and C_2C_3 distances, respectively. This results in the only qualitative difference found between the two sets of structures, in that HF leads to a methyl moiety that is still staggered to the hydride ligands, whereas, in the B3LYP-optimized geometry (Fig. 1), methyl prefers a conformation staggered to ethylene.

Agostic titanium–hydrogen interactions require the inclusion of electron correlation in order to be well described. The differences are pronounced in the γ-agostic product, for which B3LYP predicts the ethyl tail of the propyl ligand to be, on average, 10 pm closer to the metal than does Hartree–Fock. Even with such large errors for the one-particle approximation in predicting metal–ligand distances, it may be of interest to also consider intraligand distances that may be used as diagnostics of weak metal–ligand interactions. In fact, HF and B3LYP predict equal prolongation (2.1 pm) of the ethylenic CC bond upon coordination, and also a very similar lengthening ($\delta R_{agostic}$) of the carbon–hydrogen bonds of the hydrogen atoms engaged in interaction with titanium. Similar observations were reported for HF and DFT optimizations of cationic chromium(III) complexes,[53] suggesting that the description of relatively weak metal–ligand interactions may essentially be intact even if the calculated metal–ligand distances in question are too long. This is due to the softness of the relevant metal–ligand stretching modes.

Turning to the transition state region, B3LYP is seen to retain more of the ethylene π-bond than that of the Hartree–Fock model, effectively making the TS appear earlier during insertion. In contrast to the equal prolongation of the ethylene CC bond found for the coordination step, the calculated lengthenings from the π-complex to the TS are now 6.6 pm and 4.1 pm with the HF and B3LYP method, respectively. The shorter C_1—C_2 bond found with the hybrid method is accompanied by a longer computed Ti—C_1 bond, a shorter Ti—methyl bond, and a longer forming C_2—C_3 bond at the TS.

Similar observations were made in a comparison of HF- and DFT-optimized transition structures of ethylene insertion for a chromium(III) model catalyst.[53] Furthermore, in part I of this study,[1] which addresses the addition of hydrochloric acid to ethylene, inclusion of correlation effects in the geometry optimization was seen to result in an early TS retaining more of both the ethylenic π-bond and the HCl bond.

To judge the importance of the level of geometry optimization for reaction energetics, B3LYP energies were computed based on both B3LYP- and HF-optimized structures. Very similar energy profiles resulted, the difference being that HF structures led to 1 kcal/mol higher energy (relative to free reactants) for the three stationary points that display the weakest interactions between the metal and the organic ligand(s), namely the π-complex,

TS, and the γ-agostic product. Thus, the geometry effect cancels for the activation energy.

The small errors introduced in the energy profile of the reaction by using HF geometries suggest that the independent-particle level of theory may be adequate for obtaining geometries in many studies of alkene insertion in Ti(IV)-based polymerization catalysts. Results for a Cr(III) model catalyst indicate that reasonable geometries may also be expected for catalysts involving transition metals with formal electron configurations other than d^0. The effects of varying the level of geometry optimization were also seen to be limited in the first part of this study.[1] Hence, geometries obtained at the Hartree–Fock level may in fact be adequate for qualitative and even semiquantitative investigation of reactions where the dominating physical change is replacement of the ethylenic π-bond with a covalent single bond.

RELATIVE ENERGIES

Basis Set Effects at Self-Consistent-Field Levels of Theory

In part I of this study, it was demonstrated how the particularly slow approach to the Hartree–Fock limit for ethylene may lead to errors in computed overall reaction energies and, to a minor extent, also in reaction barriers. Relative energies computed with ANOM bases were found to be within 1.6 kcal/mol of corresponding Hartree–Fock limit estimates, which were computed with large ANO bases. In Table III, changes in relative energies upon improving the one-particle bases are recorded for Hartree–Fock and two gradient-corrected DFT methods. First, it may be noted that ANOM and TZD2P lead to very similar energies, probably close to the Hartree–Fock limit. On the other hand, when ANOS sets of double-ζ + polarization quality are used, distinct effects of basis set incompleteness emerge. At the HF level of accuracy, the reaction energy to the primary product is overestimated by 3.0 kcal/mol. The corresponding number taken from part I for the addition of HCl to ethylene, to produce chloroethane, is 2.8 kcal/mol. This illustrates well the generality of the conclusions reached in part I with regard to basis set effects. Turning to the DFT-based methods, the agreement between the two lower rows in Table III shows that the hybrid B3LYP method suffers from a basis set sensitivity similar to that of the pure DFT method, BPW91. Furthermore, even larger changes in relative energies are seen for these methods than HF as the basis sets are changed. The change in computed π-complexation energy serves well to illustrate this. Whereas the basis set effect of this quantity is negligible when HF is considered, a differential effect of 2 kcal/mol is observed for BPW91 and B3LYP upon trading TZD2P for ANOS. It is tempting to relate this to the difference in distance from the metal, but the independent particle basis set effect for the π coordination is still negligible when using B3LYP-optimized geometries. If the reaction profile is followed to the primary product, basis set effects found for DFT-based methods are seen to parallel those found for HF, albeit shifted by approximately 2 kcal/mol. Thus, it appears that the basis set effect related to the breaking of the π-bond in ethylene is present in both HF and DFT methods. In addition, there may be present a BSSE-induced stabilization of some 2 kcal/mol in the DFT/ANOS description of the ethylene–metal interaction, which is removed when TZD2P bases are intro-

TABLE III.
Differential Basis Set Effects of Energies (kcal / mol) Given Relative to Separated Reactants, of Ethylene Insertion for $TiH_2CH_3^+$.[a]

Method[b]	π-Complex	TS of insertion	γ-Agostic product	β-Agostic product	Nonagostic product
ΔE(RHF; ANOM)	−0.2	0.2	0.0	−0.1	−0.3
ΔE(RHF; ANOS)	−0.1	−2.1	−3.1	−3.3	−3.2
ΔE(BPW91; ANOS)	−2.1	−3.5	−4.8	−3.7	−3.9
ΔE(B3LYP; ANOS)	−2.3	−3.8	−5.2	−4.1	−4.2

[a]The RHF energies are obtained with RHF-optimized geometries. The other energies are reported for B3LYP-optimized geometries.
[b]All energy differences are computed with respect to energies obtained with the indicated method and TZD2P bases; thus, for the first entry in the table, ΔE(RHF, ANOM, π-complex) = [E(RHF, ANOM, π-complex) − E(RHF, ANOM, reactants)] − [E(RHF, TZD2P, π-complex) − E(RHF, TZD2P, reactants)].

duced. Basis set superposition errors of ~ 2 kcal/mol were reported for ethylene coordination to $TiCl_2CH_3^+$ by Axe and Coffin[12] using gradient-corrected DFT in conjunction with basis sets similar to ANOS in quality. Finally, the differences between HF- and the DFT-based methods are smaller for the β- and nonagostic products, probably due to less secondary interaction with the metal.

REACTION ENERGY PROFILE

In this subsection, a number of quantum chemical methods will be compared with respect to prediction of relative energies of the stationary points relevant to direct insertion of ethylene into the titanium–methyl bond in $TiH_2CH_3^+$. To qualify the various methods, energies are compared with a set of values referred to as "best estimates." This set is prepared by extrapolation of CCSD(T) energies according to the PCI-X scheme of Siegbahn et al.,[42] with $X = 85$ as derived in "Computational Details."

Hartree–Fock theory is not a serious contestant when it comes to computing energy profiles of reactions involving transition metals. This is apparent also from Figure 2, where both restricted and unrestricted Hartree–Fock theories are seen to overestimate severely the barrier to ethylene insertion. Even though this is, to a large extent, remedied in the spin-projected method, it is at the expense of severely underestimating the contribu-

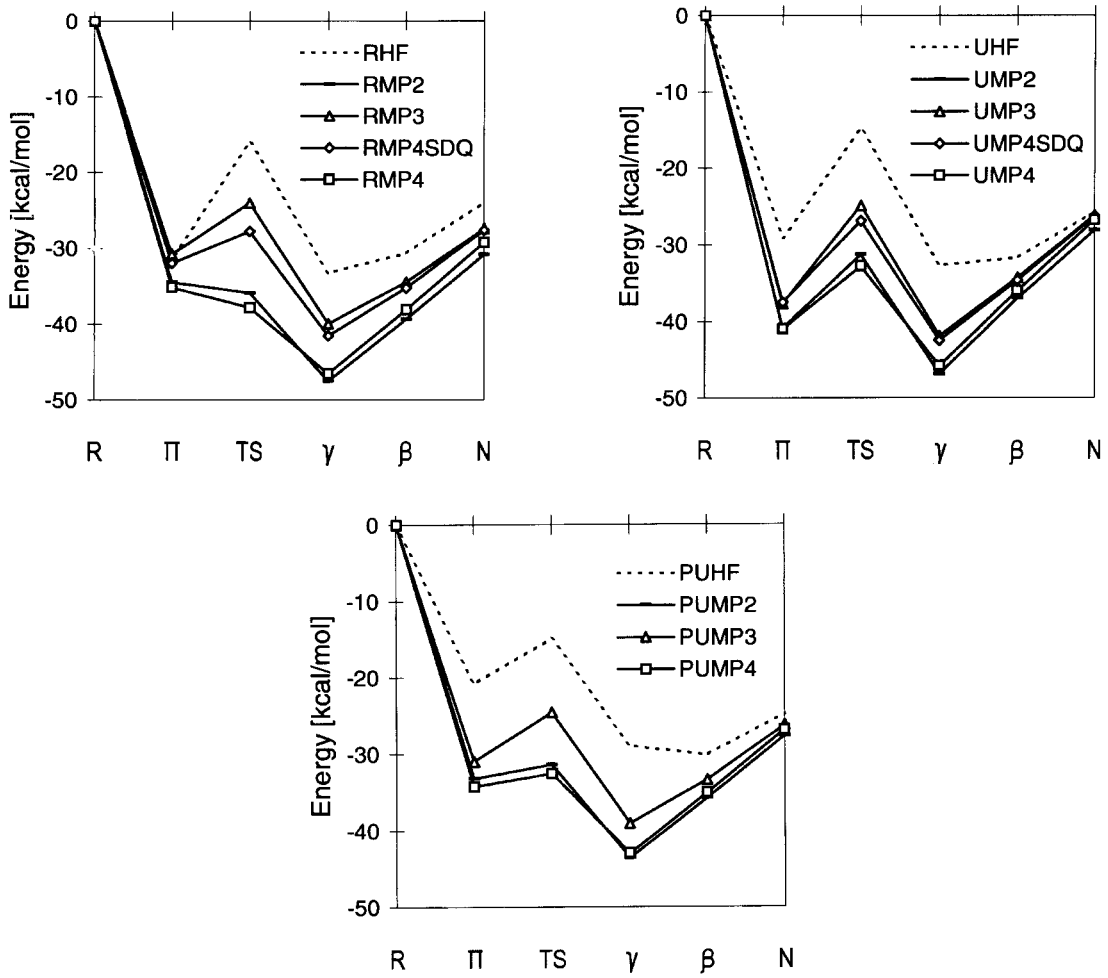

FIGURE 2. Energies of selected structures along the reaction path for insertion of ethylene into the Ti — C bond in $TiH_2CH_3^+$ as evaluated using restricted HF and MPn (upper left), unrestricted HF and MPn (bottom), and spin-projected HF and MPn (upper right). All energies are shown relative to reactants, and the structures are denoted by R (reactants); Π (π-complex), TS (transition state), γ (γ-agostic product), β (β-agostic product), and N (nonagostic product). Lines are drawn between successive points to guide the eye.

tion from weak hydrocarbon-to-metal interactions. It should be noted that the effect of spin projection is a major one for the present system, in line with the observation made by Yoshida et al. that severe spin contamination occurs in the UHF description of the metal–alkyl bond in a related system.[7] The RHF wave function suffers from a triplet instability connected to this bond. The instability with respect to lifting of spin symmetry was observed in all the current Ti complexes.

In Møller–Plesset (MP) perturbation theory, a HF determinant makes up the zeroth order wave function. In the upper leftmost part of Figure 2, energy profiles, as computed using restricted MP theory up through the fourth order, are depicted for the reaction under study. Large changes are observed following the addition of each consecutive order of correction, the fourth order corrections being almost as large as those of the third order, albeit in the opposite direction. This makes the RMP4 energy differences come out close to those obtained with only second order corrections. On the other hand, omitting the triply excited configurations to produce the popular RMP4SDQ estimate renders the relevant energy differences close to their RMP3 values. It is, in fact, difficult to detect a pattern of convergence in this perturbation series, and an extrapolation procedure like the [1, 1] Padé approximation[54] is not able to correct this situation. This does not imply that the RMPn methods are useless for the present and related systems, but rather that comparisons with more accurate methods are required to decide upon the optimal point to truncate the perturbation series. This issue will be addressed shortly. However, first one may note that the comments made with regard to restricted MP applies equally well to both the unrestricted and spin-projected MP series (cf. Fig. 2).

In the upper half of Figure 3, relative energies derived at various second order MP levels of theory are compared to our best valence-correlated values. A reasonable agreement between the various MP2 energies, and between MP2 energies and our best valence-correlated energies, is observed. Furthermore, our results show that the spin-projected PMP2 energies are particularly satisfactory, with a maximum departure from ''best'' energies less than 1.3 kcal/mol. Based on this result and the observed lack of convergence in the low-order MP series, spin-projected Møller–Plesset theory of the second order seems to be a favorable choice among the low-order MP methods. For reference purposes, Table IV provides reaction energy data as computed with various MP- and CI-based methods, including valence correlation effects only.

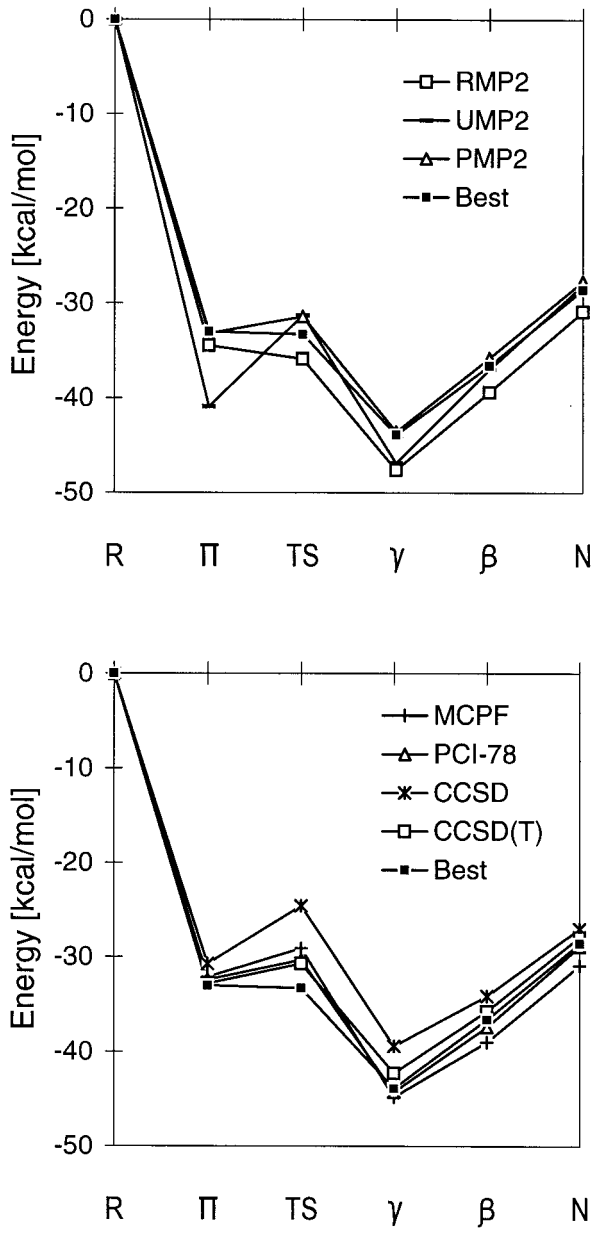

FIGURE 3. Energies of selected structures along the path for insertion of ethylene into the Ti — C bond in $TiH_2CH_3^+$ as evaluated using various MP2 methods (upper), or CI-based methods (lower). All energies are shown relative to reactants and the abscissa is labeled as in Figure 2.

TABLE IV.
Valence-Correlated Energies (kcal / mol) of Ethylene Insertion for $TiH_2CH_3^+$.[a]

Method	$D_e(\pi)$	E_{act}	$-E_{rxn}$ γ-Agostic	$-E_{rxn}$ β-Agostic	$-E_{rxn}$ Non-agostic
RMP2	34.5	−1.4	47.6	39.4	30.9
UMP2	40.9	9.6	46.9	37.0	28.1
PMP2	33.2	1.8	43.6	35.8	27.7
PMP3	31.0	6.4	39.1	33.4	26.3
PMP4	34.3	1.7	43.0	35.1	26.9
MCPF	32.1	3.0	44.8	39.0	30.9
CCSD(T)	32.8	2.1	42.3	35.7	27.9
CCSD	30.7	6.1	39.4	34.1	27.0
Best[b]	33.0	−0.3	43.9	36.6	28.6

[a] $D_e(\pi)$ is the π-complexation energy, E_{act} the energy required to reach TS from the π-complex, and $-E_{rxn}$ denotes the decrease in energy from separated reactants to various conformations of the product. Energies calculated using TZD2P bases except for MCPF, which was computed with ANOS sets. All geometries optimized at the B3LYP level.
[b] PCI-85 based on CCSD(T) energies with electron correlation included for valence electrons only.

Next, the performance of size-consistent CI-based methods is considered. Energies shown in the lower half of Figure 3 are computed with TZD2P bases, except for the MCPF method. The latter is used in conjunction with rather modest basis sets (ANOS), and aspires to high accuracy only after extrapolation of correlation effects. Such an extrapolation is carried out to create the PCI-78 entry, which also includes corrections of Hartree–Fock energies to meet the TZD2P standard. Even though PCI-78 represents a minor correction for the present reaction, it is of interest to note that it improves upon simple MCPF energies at all stationary points. Both MCPF and PCI-78 energies compare favorably with our best relative energies, although the reaction barrier is somewhat overestimated, at 3.0 and 2.5 kcal/mol, respectively, to be compared with 0.3 kcal/mol (best valence-correlated estimate). This tendency is found also for the coupled cluster methods, CCSD and CCSD(T). The CCSD method overestimates the barrier by 6 kcal/mol, and, furthermore, underestimates the stability of the products, in particular the primary γ-agostic product. Inclusion of a perturbative estimate of the contribution from triply excited configurations, to form CCSD(T) energies, is clearly needed to obtain accurate energies. Based on the use of the QCISD approximation (quadratic CI with singles and doubles, essentially CCSD lacking some terms involving single excitation amplitudes) as a reference method, Yoshida et al.[7] suggested that barriers to insertion obtained at the MP2 and DFT levels were underestimated. The modest performance of CCSD seen among our results, however, questions the correctness of using the even simpler QCISD method as reference, and indicates that both the MP2 and DFT results in ref. 7 may, in fact, be more accurate than the ones obtained with QCISD.

The effect on relative energies from choosing an unrestricted instead of a restricted reference state in the coupled-cluster calculations is very small, despite the large differences between RHF and UHF energy profiles. The stability of the transition state (relative to free reactants) is virtually unchanged between RCCSD and UCCSD, and it is changed by only 0.5 kcal/mol upon going from RCCSD(T) to UCCSD(T).

In Table V, relative energies are listed for a number of DFT and hybrid HF–DFT methods. These methods include core–core and core–valence correlation and, to provide a fair comparison, BSSE-corrected estimates of effects of including Ti $3s, 3p$ electrons in the correlation treatment have been prepared for the *ab initio* methods also in-

TABLE V.
Energies (kcal / mol) of Ethylene Insertion for $TiH_2CH_3^+$.[a]

Method	$D_e(\pi)$	E_{act}	$-E_{rxn}$ γ-Agostic	$-E_{rxn}$ β-Agostic	$-E_{rxn}$ Non-agostic
DFT and hybrid methods					
LSDA	39.9	−12.0	65.1	53.0	42.7
BP86	33.3	−3.2	46.4	38.7	30.6
BPW91	32.2	−2.7	45.2	38.0	30.0
BLYP	31.2	1.4	37.2	31.5	24.4
B3P86	33.6	−1.7	48.3	40.7	32.6
B3PW91	32.4	−0.8	46.1	39.1	31.1
B3LYP	31.7	2.4	40.0	34.1	26.8
ab initio methods[b]					
PCI-78	34.6	0.5	47.6	39.1	29.7
PMP2	34.4	0.0	45.9	36.8	28.1
Best	35.2	−2.0	47.2	38.3	29.3

[a] See Table IV for definition of symbols. Energies calculated using TZD2P bases except for PCI-78, which is based on MCPF and ANOS sets. All geometries optimized at the B3LYP level.
[b] Estimates of Ti $3s$, $3p$ correlation energies included.

cluded in Table V. It may, however, be noted that the core-correlation effects are minor for the present system, reaching a maximum of 4 kcal/mol for the transition state (relative to free reactants).

The LDA method is included for completeness, and it is clearly without interest when it comes to computing the reaction profile. Replacing the Becke 1988 exchange functional with his hybrid functional, B3, which also includes a component of correlation functional, systematically leads to destabilization of the free reactants, relative to all product conformers. This effect is not very large, varying between 0.9 and 2.8 kcal/mol among the correlation functionals and different conformers. Much larger changes are brought about when different correlation functionals are considered. The LYP functional systematically underestimates the stability of the assembled structures, thus becoming a less extreme counterpart to LSDA. Only the LYP correlation functional predicts a nonvanishing barrier to insertion from the π complex, and overall reaction energies are 5–8 kcal/mol lower for all product conformers than those obtained by the other gradient-corrected methods. As for the PW91 and P86 functionals, relative energies are obtained in good agreement with our best estimates. It is worth noting that, for methods based on these functionals, the introduction of Hartree–Fock exchange, as in the B3 methods, generally leads to departure from the best estimate values, rather than improvement. The main difference between our best energy estimates, on the one hand, and those derived by means of BP86 or BPW91, on the other, is a slight underestimation of the stability of the π-complex, of 1.9 and 3.0 kcal/mol, respectively. The BP86 functional is therefore seen to have the best overall performance among the DFT-based methods considered here.

In general, there seems to be good agreement between results obtained with perturbation theory to the second and fourth order, gradient-corrected density functional theory, and our best configuration interaction-based methods. It is gratifying that a similar pattern of agreement was obtained for the barrier to insertion in the $ZrCl_2CH_3^+$ model catalyst by Sakaki et al., as presented in ref. 43 in the study by Yoshida et al.[7] The discussion has so far drawn particular attention to four different methods that compare well with respect to accuracy and computational cost: PMP2, PCI-78 based on MCPF, and two pure DFT methods (BP86 and BPW91) (cf. Fig. 4). Considering the accuracy achieved for the present system only, and the

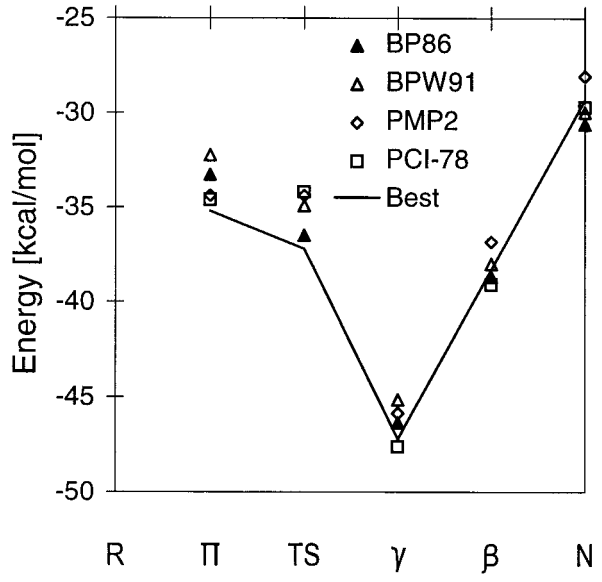

FIGURE 4. Energies of selected structures along the path for insertion of ethylene into the Ti-C bond in $TiH_2CH_3^+$, as evaluated using the methods found to give the best description of the reaction. All energies are shown relative to reactants, and the abscissa is labeled as in Figure 2.

confidence that may be put into our best-estimate energies, it is not possible to rank these methods to any further extent. However, the DFT-based methods have a distinct advantage in the ease with which core-correlation effects are included. Our results thus lend support to the approach by which Ziegler and his group obtain relative energies in their series of DFT investigations of olefin insertion reactions (see, e.g., refs. 3–5).

On the other hand, obtaining estimates of core-correlation effects when using *ab initio* methods is a difficult task. Large basis set superposition errors will be present unless the basis set is specifically designed for correlating the core region. For example, Axe and Coffin[12] reported a BSSE of 9.5 kcal/mol in the binding energy of ethylene in $TiCl_2CH_3(C_2H_4)^+$ obtained at the MP2 level with all electrons correlated. They used a $[5s5p2d]$ contracted set on Ti, and 6-31G(d, p) sets on the other atoms, which are comparable to basis sets commonly used in studies of olefin insertion reactions. If estimates of BSSE are not obtained in these cases, correlation of core electrons should be avoided in the first place as the errors introduced by the latter approach will be smaller than the BSSE. Predicted barriers to insertion (or monotoni-

cally downhill insertion, as reported in ref. 11) based on *ab initio* calculations involving correlation of core electrons without addressing the aforementioned problems, thus appears to be questionable. The inferior relative energies obtained with LDA in the present work show that previous reports based on this method[8, 11] may also be questioned. In fact, in the work by Weiss et al.[11] it is seen that the predictions by LDA and full-correlation MP2 group together. This demonstrates the overestimated stability of assembled structures obtained from full-correlation MP2 with standard basis sets. Perhaps the most obvious result of the latter effect is their unrealistically large overall insertion energies.

Acknowledgment

The authors are grateful for the extensive grants of computing time from the Research Council of Norway (Programme for Supercomputing).

References

1. K. J. Børve and V. R. Jensen, *J. Chem. Phys.*, **105**, 6910 (1996).
2. D. G. Musaev, R. D. J. Froese, M. Svensson, and K. Morokuma, *J. Am. Chem. Soc.*, **119**, 367 (1997).
3. L. Deng, P. Margl, and T. Ziegler, *J. Am. Chem. Soc.*, **119**, 1094 (1997).
4. T. K. Woo, P. M. Margl, J. C. W. Lohrenz, P. E. Blöchl, and T. Ziegler, *J. Am. Chem. Soc.*, **118**, 13021 (1996).
5. J. C. W. Lohrenz, T. K. Woo, and T. Ziegler, *J. Am. Chem. Soc.*, **117**, 12793 (1995).
6. V. R. Jensen, K. J. Børve, and M. Ystenes, *J. Am. Chem. Soc.*, **117**, 4109 (1995).
7. T. Yoshida, N. Koga, and K. Morokuma, *Organometallics*, **14**, 746 (1995).
8. R. J. Meier, G. H. J. van Doremaele, S. Iarlori, and F. Buda, *J. Am. Chem. Soc.*, **116**, 7274 (1994).
9. T. K. Woo, L. Fan, and T. Ziegler, *Organometallics*, **13**, 2252 (1994).
10. H. Weiss, F. Haase, and R. Ahlrichs, *Chem. Phys. Lett.*, **194**, 492 (1992).
11. H. Weiss, M. Ehrig, and R. Ahlrichs, *J. Am. Chem. Soc.*, **116**, 4919 (1994).
12. F. U. Axe and J. M. Coffin, *J. Phys. Chem.*, **98**, 2567 (1994).
13. Y. W. Alelyunas, R. F. Jordan, S. F. Echols, S. L. Borkowsky, and P. K. Bradley, *Organometallics*, **10**, 1406 (1991).
14. J. J. Eisch, K. R. Caldwell, S. Werner, and C. Krüger, *Organometallics*, **10**, 3417 (1991).
15. X. Yang, C. L. Stern, and T. J. Marks, *J. Am. Chem. Soc.*, **113**, 3623 (1991).
16. H. Kawamura-Kuribayashi, N. Koga, and K. Morokuma, *J. Am. Chem. Soc.*, **114**, 2359 (1992).
17. L. Fan, D. Harrison, L. Deng, T. K. Woo, D. Swerhone, and T. Ziegler, *Can. J. Chem.*, **73**, 989 (1995).
18. P. Cossee, *J. Catal.*, **3**, 80 (1964).
19. D. T. Laverty and J. J. Rooney, *J. Chem. Soc. Faraday Trans.*, **79**, 869 (1983).
20. M. Brookhart and M. L. H. Green, *J. Organomet. Chem.*, **250**, 395 (1983).
21. M. Brookhart and M. L. H. Green, *Prog. Inorg. Chem.*, **36**, 1 (1988).
22. R. Ditchfield, W. J. Hehre, and J. A. Pople, *J. Chem. Phys.*, **54**, 724 (1971).
23. W. J. Hehre, R. Ditchfield, and J. A. Pople, *J. Chem. Phys.*, **56**, 2257 (1972).
24. A. J. H. Wachters, *J. Chem. Phys.*, **52**, 1033 (1970).
25. R. C. Raffenetti, *J. Chem. Phys.*, **58**, 4452 (1973).
26. J. Almlöf and P. R. Taylor, *J. Chem. Phys.*, **86**, 4070 (1987).
27. S. Huzinaga, *J. Chem. Phys.*, **42**, 1293 (1965).
28. C. W. Bauschlicher Jr., S. R. Langhoff, and L. A. Barnes, *J. Chem. Phys.*, **91**, 2399 (1989).
29. T. H. Dunning, *J. Chem. Phys.*, **55**, 716 (1971).
30. K. Pierloot, B. Dumez, P.-O. Widmark, and B. O. Roos, *Theor. Chim. Acta*, **90**, 87 (1995).
31. M. W. Schmidt, K. K. Baldridge, J. A. Boatz, S. T. Elbert, M. S. Gordon, J. H. Jensen, S. Koseki, N. Matsunaga, K. A. Nguyen, S. J. Su, T. L. Windus, M. Dupuis, and J. A. Montgomery, *J. Comput. Chem.*, **14**, 1347 (1993).
32. M. J. Frisch, G. W. Trucks, H. B. Schlegel, P. M. W. Gill, B. G. Johnson, M. A. Robb, J. R. Cheeseman, T. Keith, G. A. Petersson, J. A. Montgomery, K. Raghavachari, M. A. Al-Laham, V. G. Zakrzewski, J. V. Ortiz, J. B. Foresman, C. Y. Peng, P. Y. Ayala, W. Chen, M. W. Wong, J. L. Andres, E. S. Replogle, R. Gomperts, R. L. Martin, D. J. Fox, J. S. Binkley, D. J. Defrees, J. Baker, J. P. Stewart, M. Head-Gordon, C. Gonzalez, and J. A. Pople, *Gaussian-94*, Gaussian, Inc. Pittsburgh, PA, 1995.
33. C. Møller and M. S. Plesset, *Phys. Rev.*, **46**, 618 (1934).
34. D. P. Chong and S. R. Langhoff, *J. Chem. Phys.*, **84**, 5606 (1986).
35. *Stockholm* is a general purpose quantum chemical set of programs written by P. E. M. Siegbahn, M. R. A. Blomberg, L. G. M. Pettersson, B. O. Roos and J. Almlöf. Contact Prof. Per E. M. Siegbahn, Department of Physics, University of Stockholm, Sweden, for more information.
36. J. A. Pople, R. Krishnan, H. B. Schlegel, and J. S. Binkley, *Int. J. Quantum Chem.*, **XIV**, 545 (1978).
37. J. Cizek, *Adv. Chem. Phys.*, **14**, 35 (1969).
38. G. D. Purvis and R. J. Bartlett, *J. Chem. Phys.*, **76**, 1910 (1982).
39. G. E. Scuseria, C. L. Janssen, and H. F. Schaefer III, *J. Chem. Phys.*, **89**, 7382 (1988).
40. G. E. Scuseria and H. F. Schaefer III, *J. Chem. Phys.*, **90**, 3700 (1989).
41. J. A. Pople, M. Head-Gordon, and K. Raghavachari, *J. Chem. Phys.*, **87**, 5968 (1987).

42. P. E. M. Siegbahn, M. R. A. Blomberg, and M. Svensson, *Chem. Phys. Lett.*, **223**, 35 (1994).
43. P. E. M. Siegbahn, M. Svensson, and P. J. E. Boussard, *J. Chem. Phys.*, **102**, 5377 (1995).
44. Ø. Espelid and K. J. Børve, *J. Phys. Chem. A*, **101**, 9449 (1997).
45. J. C. Slater, *The Self-Consistent Field for Molecular and Solids, Vol. 4*, McGraw-Hill, New York, 1974.
46. S. H. Vosko, L. Wilk, and M. Nusair, *Can. J. Phys.*, **58**, 1200 (1980).
47. A. D. Becke, *Phys. Rev. A*, **38**, 3098 (1988).
48. C. Lee, W. Yang, and R. G. Parr, *Phys. Rev. B*, **37**, 785 (1988).
49. J. P. Perdew, *Phys. Rev. B*, **33**, 8822 (1986).
50. J. P. Perdew and Y. Wang, *Phys. Rev. B*, **45**, 13244 (1992).
51. W. Meyer and P. Rosmus, *J. Chem. Phys.*, **63**, 2356 (1975).
52. L. G. M. Pettersson and H. Åkeby, *J. Chem. Phys.*, **94**, 2968 (1991).
53. V. R. Jensen and K. J. Børve, *Organometallics*, **16**, 2514 (1997).
54. Z. He and D. Cremer, *Int. J. Quantum Chem.*, **59**, 71 (1996).